Respiratory Research

RESEARCH Open Access

The role and mechanism of thrombospondin-4 in pulmonary arterial hypertension associated with congenital heart disease

Haowei Zeng[1], Beidi Lan[1], Bingyi Li[1], Hang Xie[1], Enfa Zhao[2], Xiaoqin Liu[1], Xiaoyi Xue[1], Jingyan Sun[1], Linjie Su[1] and Yushun Zhang[1*]

Abstract

Background Due to a special hemodynamic feature, pulmonary vascular disease in pulmonary arterial hypertension associated with congenital heart disease (PAH-CHD) has two stages: reversible and irreversible. So far, the mechanism involved in the transition from reversible to irreversible stage is elusive. Moreover, no recognized and reliable assessments to distinguish these two stages are available. Furthermore, we found that compared with control and reversible PAH, thrombospondin-4 (THBS4) was significantly upregulated in irreversible group by bioinformatic analysis. Hence, we further verify and investigate the expression and role of THBS4 in PAH-CHD.

Methods We established the monocrotaline plus aorto-cava shunt-induced (MCT-AV) rat model. We measured the expression of THBS4 in lung tissues from MCT-AV rats. Double immunofluorescence staining of lung tissue for THBS4 and α-SMA (biomarker of smooth muscle cells) or vWF (biomarker of endothelial cells) to identify the location of THBS4 in the pulmonary artery. Primary pulmonary artery smooth muscle cells (PASMCs) were cultivated, identified, and used in this study. THBS4 was inhibited and overexpressed by siRNA and plasmid, respectively, to explore the effect of THBS4 on phenotype transformation, proliferation, apoptosis, and migration of PASMCs. The effect of THBS4 on pulmonary vascular remodeling was evaluated in vivo by adeno-associated virus which suppressed THBS4 expression. Circulating level of THBS4 in patients with PAH-CHD was measured by ELISA.

Results THBS4 was upregulated in the lung tissues of MCT-AV rats, and was further upregulated in severe pulmonary vascular lesions. And THBS4 was expressed mainly in PASMCs. When THBS4 was inhibited, contractile markers α-SMA and MYH11 were upregulated, while the proliferative marker PCNA was decreased, the endothelial-mensenchymal transition marker N-cad was downregulated, proapototic marker BAX was increased. Additionally, proliferation and migration of PASMCs was inhibited and apoptosis was increased. Conversely, THBS4 overexpression resulted in opposite effects. And the impact of THBS4 on PASMCs was probably achieved through the regulation of the PI3K/AKT pathway. THBS4 suppression attenuated pulmonary vascular remodeling. Furthermore, compared with patients with

*Correspondence:
Yushun Zhang
zys2889@sina.com

Full list of author information is available at the end of the article

simple congenital heart disease and mild PAH-CHD, the circulating level of THBS4 was higher in patients with severe PAH-CHD.

Conclusions THBS4 is a promising biomarker to distinguish reversible from irreversible PAH-CHD before repairing the shunt. THBS4 is a potential treatment target in PAH-CHD, especially in irreversible stage.

Keywords Congenital heart disease, Pulmonary arterial hypertension, Pulmonary vascular remodeling, Reversibility, Thrombospondin-4

Introduction

The prevalence of pulmonary artery hypertension associated with congenital heart disease (PAH-CHD) is $(1.6–12.5)/10^6$ [1, 2]. Three to seven percent of adult patients with congenital heart disease (CHD) and 3% of patients after defect closure will develop pulmonary artery hypertension (PAH) [3]. Two to six percent of children with CHD whose pulmonary lesion will accelerate after CHD closure [4]. Due to its unique hemodynamics, pulmonary vascular disease in PAH-CHD can generally be reversed in an early phase, timely closure of the shunt during this period will cause normalization of pulmonary hemodynamics and vascular morphology, however, PAH-CHD with systemic-to-pulmonary shunt can ultimately become irreversible, closure of the shunt during this period will accelerate disease progression, as these patients have the worst prognosis among other PAH-CHD types [5–7]. Unfortunately, to date, the mechanism involved in the transition from reversible to irreversible stage is elusive. Moreover, no recognized and reliable assessments to distinguish these two stages are available. Hence, it is of major clinical importance to identify biomarkers to distinguish these two stages and elucidate the mechanisms involved in the transition from reversible stage to the irreversible stage in PAH-CHD.

Thrombospondin-4 (THBS4) is one of the members of the extracellular matrix protein-thrombospondin family. THBS4 improves angiogenesis. THBS4 is among the top 1% of the most upregulated genes in gastric cancer and breast cancer [8–10]. THBS4 is also involved in the progression of prostate cancer, hepatocellular carcinoma, and bladder cancer [11–16]. Vascular endothelial cells and smooth muscle cells express THBS4. And THBS4 is usually located on the outer side of the capillaries and in the adventitia of a large blood vessel [17]. Human endothelial cells and vascular smooth muscle cells of brain blood vessels and coronary arteries also express THBS4, and THBS4 improves the proliferation of endothelial cells and vascular smooth muscle cells [18]. Studies in vitro and in vivo showed that THBS4 promotes growth of vascular cells, angiogenesis, and vascular remodeling [17, 19–22]. Compared with wide-type mice, $THBS4^{-/-}$ mice showed reduced angiogenesis and reduced adhesion, proliferation, and migration of endothelial cells. Conversely, recombinant THBS4 promotes the migration and proliferation of endothelial cells [17, 20].

Bioinformatic analysis of the monocrotaline plus aortocaval shunt induced (MCT-AV) rat model showed that compared with the control and reversible groups, THBS4 was significantly elevated in the irreversible groups. However, the role of THBS4 in PAH is unknown. Given the fact that THBS4 promotes the tumor progression and promotes proliferation of smooth muscle cells, we speculate that THBS4 plays a vital role in PAH-CHD, and THBS4 will be a promising biomarker and therapeutic target.

Herein, we investigate the expression and location of THBS4 in lung tissues from the MCT -AV rat model. THBS4 was inhibited and overexpressed by siRNA and plasmid, respectively, to explore the effect of THBS4 on the phenotype transformation, proliferation, apoptosis, and migration of pulmonary artery smooth muscle cells (PASMCs). The effect of THBS4 on pulmonary vascular remodeling was evaluated in vivo by adeno-associated virus (AAV) which suppressed THBS4 expression. Furthermore, we measured the circulating level of THBS4 in patients with PAH-CHD.

Methods

Dataset information and data processing

GSE149899 was downloaded from the NCBI Gene Expression Omnibus database (https://www.ncbi.nlm.nih.gov/geo/), it is based on GPL22396 llumina HiSeq 4000 (Rattus norvegicus). PAH was induced by MCT-AV. The reversibility of PAH was decided by the normalization of the morphological changes after hemodynamic unloading - transplanting the left lung of MCT-AV rats to healthy rats. It consisted of transcript profiles of lung tissues from 5 normal controls, 12 reversible PAH-CHD, and 6 irreversible PAH-CHD. Rattus_norvegicus. Rnor_6.0.103.gtf obtained from Ensembl (http://asia.ensembl.org/index.html) was used to transform the ensemble gene ID into gene symbols. Eventually, we got 21,882 mRNAs for further analysis by eliminating other types of RNA. The transcript profiles were log2 transformed and normalized to ensure that the expression levels had a similar distribution among a set of arrays using the "*limma*" package [23] in R software (*version 4.0.2;*https://www.r-project.org/).

Measurement of circulating level of THBS4 in patients with PAH-CHD by ELISA

The patients were divided into three groups: (1) Simple CHD ($n=8$); (2) Mild PAH-CHD ($n=5$): patients with PAH-CHD but who can still repair the shunt; (3) Severe PAH-CHD ($n=5$): patients with PAH-CHD after defect repair, or Eisenmenger syndrome, or patients with PAH-CHD who can not repair the defect. When patients with PAH-CHD meet the criterion of Qp: Qs>1.5 and Rp: Rs<0.33, the defect closure should be considered. The plasma was collected from patients with CHD with or without PAH. All patients signed an informed consent. A human THBS4 ELISA kit (Cusabio, China) was used to measure the circulating level of THBS4 according to the manufacturer's instructions. Briefly, plasma was incubated in microplate-coated plates, washed, and labeled. The optical density of the wells was detected by a microplate reader at 450 nm. A standard curve was generated according to the optical density of the standard proteins, then THBS4 level of the samples was calculated according to the standard curve. Each sample was run in triplicate.

Monocrotaline plus aorto-cavashunt-induced (MCT-AV) rat model

All protocols in animal studies were approved by the Ethics Committee of Xi'an Jiaotong University (No. 2021−1510). This study was in accordance with the Guide for the Care and Use of Laboratory Animals (NIH Publication No.85−23, National Academy Press, Washington, DC, revised 2011). Sprague-Dawley rats (male, 250 g) were purchased from the animal experimental center of Xi'an Jiaotong University. Thirty rats were randomly divided into three groups: (1) control ($n=5$); (2) sham ($n=5$); (3) MCT plus AV shunt (MS) ($n=20$). The rats were kept in a 12 h light-dark cycle and received food and water ad lib. MCT-AV model were performed as previously described [24]. Briefly, MCT (MUST BIO, China) was resolved in 1 M HCL, then neutralized to pH 7.4 by 1 M NaOH and diluted to a final concentration of 18 mg/ml using distilled water. Rats were subcutaneous injected 60 mg/kg MCT or vehicle at the first day and preformed aorto-caval shunt surgery using an 18G needle or sham surgery at eighth day. Lung tissues and heart were harvested 1, 2, 3, 4 weeks after the shunt surgery, respectively.

Hemodynamic measurements

The right ventricular systolic pressure (RVSP) was measured three weeks after the AV shunt. In brief, a heparin-priming polyethylene catheter connected to PowerLab 16/30 was inserted into the right jugular vein and advanced into the right ventricle and the main pulmonary artery.

Rat tissue collection

The heart and lungs were rapidly collected and weighted after anesthesia. Right heart hypertrophy was assessed by right heart hypertrophy index (RVHI, also known as the Fulton index, RVHI is calculated as the weight ratio of the right ventricle and left ventricle plus interventricular septum) and weight ratio of right heart and total weight. The heart and left lung were cut into appropriate size and fixed in 10% neutral formalin, dehydrated and embedded with paraffin for immunohistochemistry (IHC) staining, immunofluorescence (IF) staining, and hematoxylin and Eosin (HE) staining. The right lung was frozen at -80 ℃ for qRT-PCR and western blot analysis.

Immunohistochemistry (IHC) staining

Paraffin-embedded lung tissues were cut into 5 μm-thick sections, deparaffinized, and rehydrated. After heating in citrate buffer (pH 6.0) for antigen retrieval, 3% H_2O_2 was used to block endogenous peroxidase, then goat serum was used to block nonspecific binding. The lung sections were then incubated with primary antibody against α-SMA (Proteintech, China, 1:2500) overnight at 4 ℃ and secondary antibody 1 h at room temperature. Finally, the color reaction was completed by 3, 3′-diaminobenzidine (DAB, Servicebio, China) as chromogenic substrate. Hematoxylin was used to counterstain the nucleus. IHC slides were masked with resin and analyzed under an inverted microscope.

Immunofluorescence (IF) staining

Paraffin-embedded lung tissues were cut into 5 μm-thick sections, deparaffinized, and rehydrated. After heating in citrate buffer (pH 6.0) for antigen retrieval, goat serum was used to block nonspecific binding. The lung sections were then incubated with primary antibodies against THBS4 (Abcam, America, 1:100), α-SMA (Proteintech, China, 1:2500), and Vwf (SANTA CRUZ, America, 1:50) overnight at 4 ℃ and secondary antibody 1 h at room temperature (protected from light). Finally, DAPI was used to counterstain the nucleus. IF slides were rapidly analyzed under a fluorescence microscope.

Morphological evaluation

HE and IF staining against α-SMA of lung tissues were used to evaluate the morphological changes. The results of the α-SMA IF staining were used to evaluate the muscularization of the small pulmonary arterioles. Each lung was divided into four quadrants, ten small pulmonary arterioles (diameter<100 μm) were randomly selected per quadrant. Each arteriole was calssified as being non-muscularized, partially-muscularized (α-SMA positive in less than three-fourths of the vessel circumference), and fully-muscularized (α-SMA positive in more than three-fourths of the vessel circumference). Then the percentage

of non-muscularized, partially-muscularized, and fully-muscularized vessel was calculated. Furthermore, ten fully-muscularized vessels were randomly selected and analyzed by Image J software. The total area (TA) and lumen area (LA) were measured by Image J. Next, external diameter (ED), lumen diameter (LD), wall thickness (WT), and wall area (WA) were calculated based on TA and LA.ED = $2\sqrt{TA/\pi}$, LD = $2\sqrt{LA/\pi}$, WT = (ED-LD)/2, WT% = 2WT/ED×100%, WA% = (TA-LA)/TA×100%.

$$ED = 2\sqrt{TA}/\pi, LD = 2\sqrt{LA}/\pi$$

Primary culture of rat PASMCs

As previously described [25], the Sprague-Dawley rat (male, 100 g) was sacrificed, the heart and lungs were quickly harvested and placed in a tube with sterile iced PBS. And the pulmonary artery was separated, then all connective tissues and intima were removed, and cut into 1 mm×1 mm pieces, and cultured in a culture flask. PASMCs were cultured in DMEM/F12 (Gibco, China) containing 20% fetal bovine serum (FBS) and 1% penicillin/streptomycin in an incubator at 37 °C with 5% CO2. PASMCs which are 50-70% confluent were passaged in a ratio of 1:2−1:3. In this study, PASMCS at passages 2–4 were used. IF staining against α-SMA was used to identify PASMCs (supplementary Fig. 1).

siRNA transfection of PASMCs

The siRNA targeting for THBS4 (si-THBS4: 5'-CGAGU GACAACAGCAAAUATT-3'; 5'-UAUUUGCUGUUGU CACUCGTT-3') and control (si-CON: 5'-UUCUCCGA ACGUGUCAC GUTT-3'; 5'-ACGUGACACGUUCGG AGAATT-3') was designed and synthesized by GenePharma (shanghai, China). Cells that are 30–50% confluent were used for siRNA transfection using transfection reagent (jetPRIME®, France) according to the manufacturer's instructions. Transfection efficiency was verified by Western blot and qRT-PCR after 48 h of transfection. PASMCs were harvested for mRNA and protein expression, cell proliferation assay, apoptosis assay, and migration assay after 48 h of transfection.

Plasmid construction and transfection of PASMCs

The plasmid was designed and synthesized by GenePharma (shanghai, China) to overexpress THBS4. Cells that are 80–90% confluent were used for plasmid transfection using transfection reagent (jetPRIME®, France) according to the manufacturer's instructions. Four hours after transfection, transfection medium was replaced with fresh DMEM/F12 containing 10% FBS. Transfection efficiency was verified by Western blot and qRT-PCR after 48 h of transfection. PASMCs were harvested for mRNA and protein expression, cell proliferation assay, apoptosis assay, and migration assay after 48 h of transfection.

Cell proliferation assay

The proliferation of PASMCs was detected using the BeyoClick™ EdU-488 kit (Beyotime, China) 48 h after transfection. PASMCs were incubated with 10 μM 5-ethynyl-20-deoxyuridine (EdU) for 3 h in incubator at 37 °C with 5% CO2. After incubation, PASMCs were fixed in 10% neutral formalin for 20 min and permeabilized with 0.3% Triton X-100 for 15 min. Then, click reaction solution was added to the PASMCS for 30 min and Hoechst 33,342 was added to counterstain the nucleus. Finally, a fluorescent microscope was used to collect images. Cells with green nucleus represents EdU-positive cells, and cells with blue nucleus represents total cells. The percentage of EdU positive cells was calculated as the ratio number ratio of EdU positive cells and total cells.

Cell apoptosis assay

PASMCs apoptosis was detected by Annexin V-FITC kits (Beyotime, China) according to the manufacturer's protocol. Briefly, 48 h after transfection, PASMCs were trypsinized and washed in PBS, then resuspended with 195 μl binding buffer. Next, 5 μl FITC Annexin V and 10 μl PI were added, mixed, incubated for 20 min at room temperature (protected from light), and analyzed using flow cytometry within 1 h. PASMCs in the early stage of apoptosis stain positive for FITC Annexin V and negative for PI, whereas PASMCs in the late stage of apoptosis stain positive for FITC Annexin V as well as PI.

Cell migration assay

The wound healing assay and the Transwell assay are collectively used to assess the migration of PASMCs. Cells with 100% confluent after transfection were used for the wound healing assay. At this point, cells were scratched with a yellow pipet tip. After three times of gentle washing with PBS, the medium was replaced with DMEM/F12 containing 2% FBS and further incubated in incubator at 37 °C with 5% CO2. The images were acquired at 0 h and 24 h after scratching with an inverted microscope. Wound healing was assessed by the percentage of reduced scratching area. The percentage of reduced scratching area = (scratching area at 0 h - scratching area at 24 h)/ scratching area at 0 h.

For the Transwell assay, 200 μl PASMCs were resuspended in serum-free DMEM/F12 (a density of 5×10^4/ml, 200 μl) and added into the upper compartment of Transwell chamber (0.8 μm, Corning, America). DMEM/F12 containing 20% FBS (700 μl) were added to bottom chamber. After incubation for 24 h, non-migratory cells were removed by cotton swab gently. Then, migratory cells were fixed in 10% neutral formalin for 20 min,

stained with crystal violet for 20 min, and washed with PBS three times. The images were acquired by an inverted microscope. Ten fields were randomly selected to calculate the number of migratory cells. The result were presented as folds of the migratory cells.

Quantitative real-time polymerase chain reaction (qRT-PCR)

Total RNA was extracted from lung tissues or PASMCs using Trizol reagent (Takara, Japan) and the concentration was measured. Reverse transcription reagent kits (abm, China) were used to reverse-transcribe total RNA to cDNA. The SYBR green Universal Master Mix (Servicebio, China) was used to perform real-time PCR system according to the manufacturer's protocol. The sequences of the primers were as follows: THBS4, forward 5′-3′ CGGATGGAGACGGGATCTTG, reverse 3′-5′ GTCACAGGCATCCCCAAAGA; GAPDH forward 5′-3′ GGTGGACCTCATGGCCTACA, reverse 3′-5′ T CTCTTGCTCTCAGTATCCTTGCT. Each sample was run in triplicate. The expression levels of the mRNAs were normalized to GAPDH and calculated using the $2^{-\Delta\Delta Ct}$ method.

Western blot

RIPA was used to extract proteins from lung tissues or PASMCs. BCA protein assay was used to measure protein concentration to guarantee the equal protein amount for western blot. Proteins were separated with sodium dodecyl sulfate-polyacrylamide gel electrophoresis (SDS-PAGE) and transferred onto a polyvinylidene fluoride (PVDF) membrane. The PVDF membrane was blocked for nonspecific binding with blocking buffer and incubated with primary antibodies against THBS4 (Abcam, USA, 1:1000), GAPDH (Proteintech, China, 1:20000), α-SMA (Proteintech, China, 1:20000), MYH11 (SANTA CRUZ, America, 1:200), PCNA (SANTA CRUZ, America, 1:200), N-cad (SANTA CRUZ, America, 1:200), BAX (Abmart, China, 1:1000), AKT (CST, America,1:1000), PI3K (CST, America, 1:1000), p-AKT (Abmart, China, 1:1000), and p-PI3K (Abmart, China, 1:1000) overnight at 4 ℃. After incubation with horseradish peroxidase (HRP)-conjugated secondary antibody, protein bands were visualized using enhanced chemiluminescence plus immunoblotting detection reagents (Millipore, Boston, USA), followed by exposure to a scanning imager. Images were quantified by Image J software and normalized to GAPDH.

Adeno-associated virus (AAV) administration

AAV for silencing THBS4 and a control vector was designed and synthesize by HANBIO (shanghai, China). The target sequence of AAV2/6-EGFP-siCON was TTC TCCGAACGTGTCACGTAA with a final concentration of 1.9×10^{12} vg/ml. The target sequence of AAV2/6-EGFP-siTHBS4 was CGAGTGACAACAGCAAATA, with a final concentration of 1.8×10^{12} vg/ml. Sprague-Dawley rats (male, 200 g) were randomly divided into 4 groups: (1) control ($n=5$); (2) sham ($n=5$); (3) AAV-con and MCT-AV shunt (MS-AAV-siCON) ($n=6$); (4) AAV-siTHBS4 and MC -AV shunt (MS-AAV-siTHBS4) ($n=6$). After anesthetizing, AAV (200 μl) or PBS (200 μl) was intratracheal administrated. Next, rats were treated as described above seven days after AAV delivery.

Statistical analyses

All statistical analyses were performed by SPSS 23,0. GraphPad Prism 9 was used to draw graphs, all results are presented as mean±SD. Comparison between two groups was evaluated by Student's t test; Comparison among three or four groups was evaluated by one-way analysis of variance (ANOVA); $P<0.05$ was considered as statistically significant. All experiments were repeated at least three times.

Results

Circulating level of THBS4 in patients with PAH-CHD

Circulating level of THBS4 in simple CHD, mild PAH-CHD, and severe PAH-CHD were 73.86±15.99 ng/ml, 68.10±28.34 ng/ml, and 106.50±22.91 ng/ml, respectively. Compared with simple CHD and mild PAH-CHD, circulating levels of THBS4 in severe PAH-CHD were significantly elevated ($P=0.0466$ and $P=0.0339$, respectively) (Fig. 1).

Evaluation of MCT-AV rats model by hemodynamic parameters and morphological methods

Three weeks after AV shunt, right heart catheterization was used to evaluate the MCT-AV rat model. Compared with control, MCT-AV group showed significantly higher RVSP (Fig. 2A). HE staining of heart showed thicker right ventricular wall, higher RVHI, higher weight ratio of right heart and total weight (Fig. 2B), and larger cross-sectional area of right ventricular cardiomyocyte (Fig. 2C) in MCT-AV rat model. HE staining of lung tissues (Fig. 3A) showed significant vascular remodeling including thickened vascular wall, medial hypertrophy, muscularization of small pulmonary arterioles, neointima lesions, luminal occlusion, and infiltration of immune cells. Furthermore, α-SMA IF staining (Fig. 3B) also showed thickened vascular wall, medial hypertrophy, and muscularization of small pulmonary arterioles. As the degree of muscularization of small pulmonary arterioles (Fig. 3C-E) was classified into fully-, partially-, and non-muscularized, the percentage of fully-muscularized arterioles obviously increased and non-muscularized arterioles decreased in the MCT-AV rat model. We analyzed the vascular wall thickness (Fig. 3F) and the wall area (Fig. 3G) of

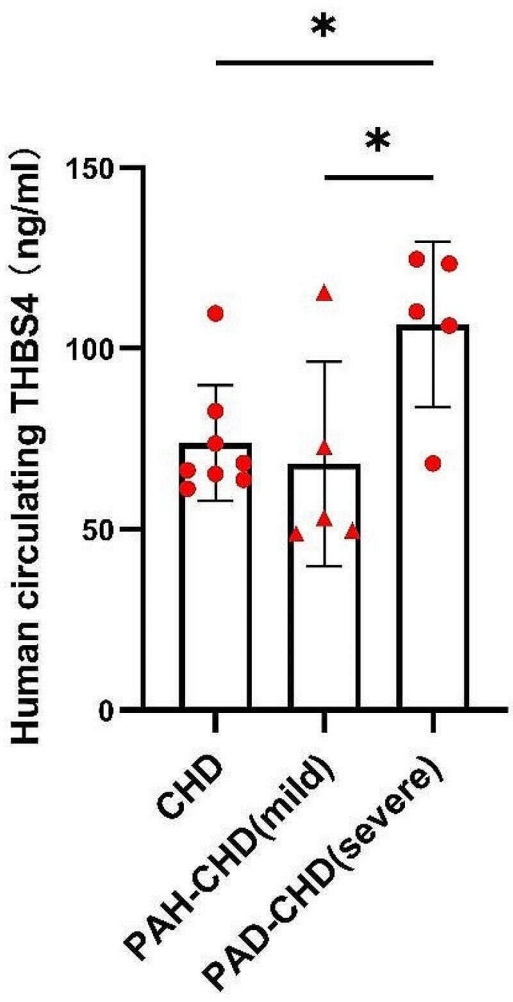

Fig. 1 Circulating level of THBS4 in patients with PAH-CHD. The resultant data are represented as mean ± SD. $^{*}P < 0.05$

fully-muscularized pulmonary arterioles, the percentage of vascular wall thickness and wall area increased and further increased with vascular lesions exacerbated.

THBS4 is up-regulated in lung tissues from MCT -AV rats

Firstly, we analyzed the dataset (GSE149899) from the GEO database (Fig. 4A). Compared with the control and the reversible group, THBS4 is significantly increased in the irreversible group ($P=0.0005$ and $P<0.0001$, respectively). Then we further verified the expression of THBS4 in MCT-AV rats. qRT-PCR (Fig. 4B) and Western blot (Fig. 4C) showed that THBS4 expression is increased and further increased with vascular lesions exacerbated.

Double IF staining of lung tissues (Fig. 4D) from MCT-AV rats and rats in control group for THBS4 and α-SMA (biomarker of PASMCs) or for THBS4 and von Willebrand Factor [VWF, biomarker of pulmonary artery endothelial cells (PAECs)] showed that both PAECs and PASMCs express THBS4, but PASMCs was the main source. At the same time, the IF staining also showed that THBS4 is upregulated in lung tissues from MCT-AV rats compared with control. Hence, we focus the following study about influence of THBS4 on PASMCs.

THBS4 induces PASMCs phenotype transformation

The transformation of phenotype is vital in PAH, so we further analyzed the effect of THBS4 on phenotype transformation of PASMCs. Inhibition and overexpression of THBS4 was achieved by siRNA transfection and plasmid transfection, respectively. Both qRT-PCR (Fig. 5A) and Western blot (Fig. 5B) showed excellent transfection efficiency. When THBS4 is inhibited, the expression of contractile markers (α-SMA and MYH11) and the pro-apoptosis marker (BAX) are increased, while the proliferative marker (PCNA), and the endothelial-mensenchymal transition marker (N-CAD) decreased. Conversely, when THBS4 is overexpressed, the expression of α-SMA, MYH11, and BAX are decreased while PCNA and N-cad are increased (Fig. 5C). Together, the result implies that THBS4 predisposes PASMC to a proliferative, apoptosis-resistant phenotype.

THBS4 promotes PASMCs proliferation

Next, we investigated the effect of THBS4 on proliferation of PASMCs by the EdU assay. The EdU assay (Fig. 6A) showed that the percentage of proliferating cells are reduced in the si-THBS4 group (3.130±0.434% vs. 4.071±0.343%, $P=0.0421$) and elevated in the pEX3-THBS4 group 16.08±2.138% vs. 9.300±0.293%, $P=0.0055$). The result is congruent with the previous expression change of the proliferation marker-PCNA. Briefly, THBS4 facilitates the proliferation of PASMCs.

THBS4 inhibits PASMCs apoptosis

The apoptosis of PASMCs was assessed by Annexin-V flow cytometry (Fig. 6B). The result showed that the early apoptosis ratio is increased (9.532%±2.833 vs. 5.584%±1.935, $P=0.0330$) when THBS4 was inhibited and decreased (5.985±0.536 vs. 8.038±0.733, $P=0.0040$) when THBS4 was overexpressed. The results were in line with the previous expression change of the pro-apoptosis marker-BAX. Collectively, THBS4 represses apoptosis of PASMCs. However, THBS4 has no obvious effect on late apoptosis of PASMCs (19.56%±2.893 vs. 18.45±5.178, $P=0.6871$, when THBS4 was inhibited and 11.78±1.283 vs. 10.12±1.583, $P=0.1548$, when THBS4 was overexpressed).

THBS4 promotes PASMCs migration

The Transwell assay (Fig. 6C) and the wound healing assay (Fig. 6D) were collectively used to assess the

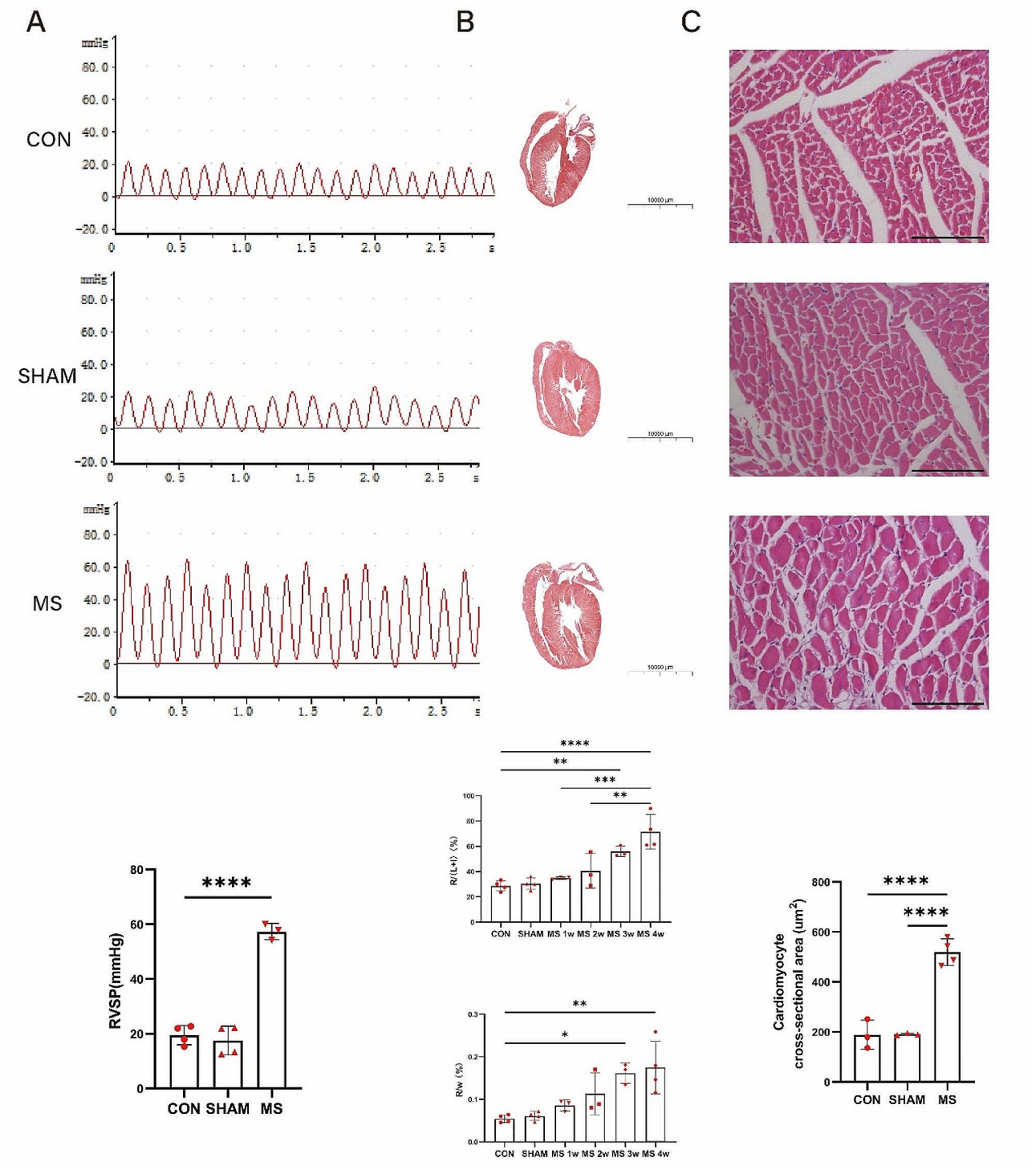

Fig. 2 Hemodynamics and right ventricular hypertrophy in the MCT plus aorto-caval shunt induced PAH rats model. **(A)** Right ventricular systolic pressure (RVSP). **(B)**Time course of the right ventricular hypertrophy index (RVHI) and weight ratio of the right heart/total weight (R/w). R: weight of the right ventricular, L + I: weight of the left ventricle and interventricular septum. Scare bars,100 μm. **(C)** Cross-sectional area of the right ventricular cardiomyocyte. Scare bars,100 μm. CON: control group; SHAM: sham group; MS: MCT plus aorto-caval shunt (MS) induced PAH rats from 1 week (1w) to 4 weeks (4w). The resultant data are represented as mean ± SD. $^{*}P < 0.05$; $^{**}P < 0.01$; $^{***}P < 0.001$; $^{****}P < 0.0001$

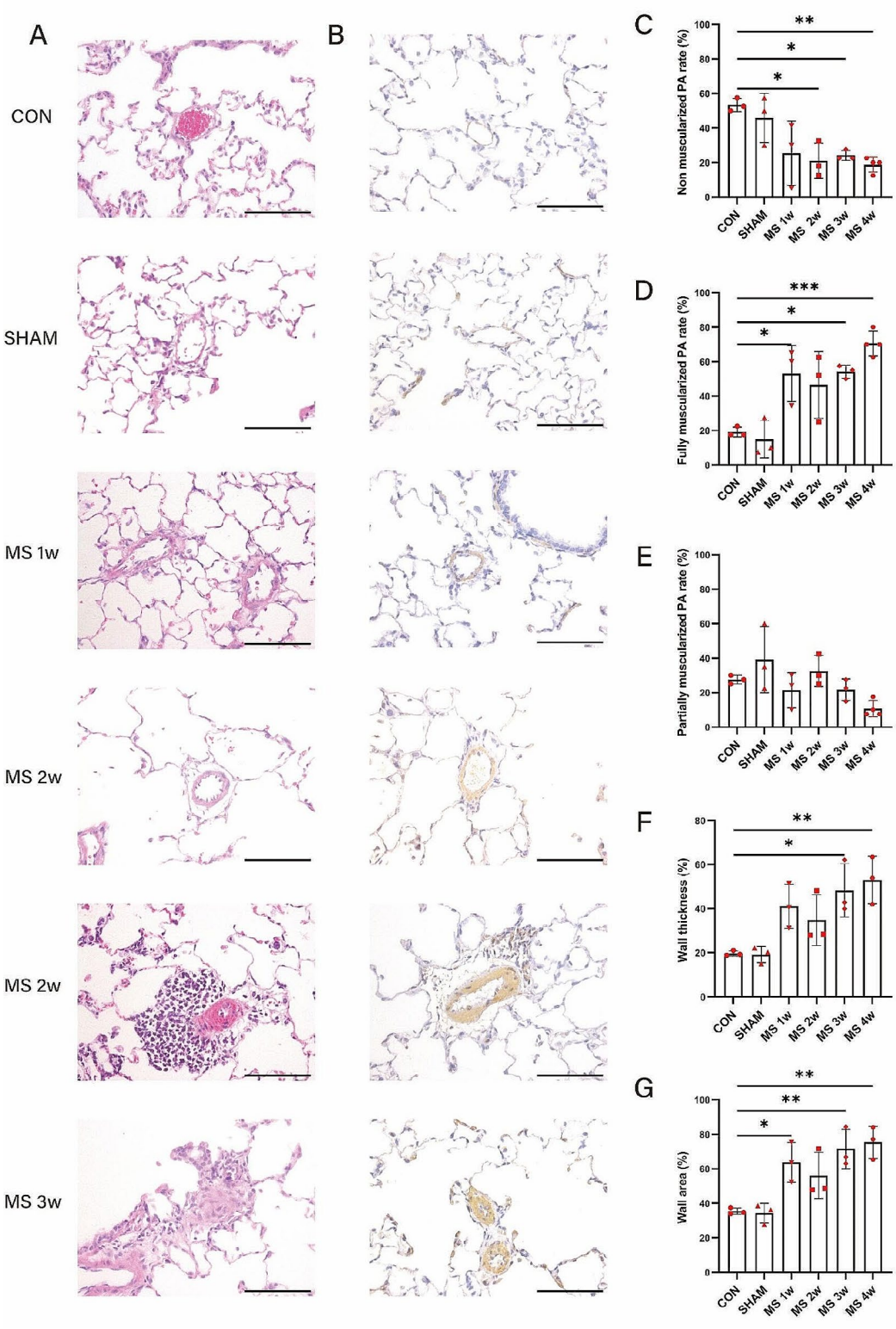

Fig. 3 Time course of morphological changes in PAH rats induced by MCT plus aorto-caval shunt. **(A)** Hematoxylin and Eosin staining of lung tissues. Scare bars,100 μm. **(B)** Immunofluorescence staining of α-SMA in lung tissues. Scare bars,100 μm. **(C)** The percentage of non-muscularized pulmonary arterioles **(D)** The percentage of partially-muscularized pulmonary arterioles. **(E)** The percentage of fully-muscularized pulmonary arterioles. **(F)** The percentage of wall thickness. **(G)** The percentage of wall area. CON: control group; SHAM: sham group; MS: MCT plus aorto-caval shunt (MS) induced PAH rats from 1 week (1w) to 4 weeks (4w). The resultant data are represented as mean ± SD. $^{*}P < 0.05$; $^{**}P < 0.01$

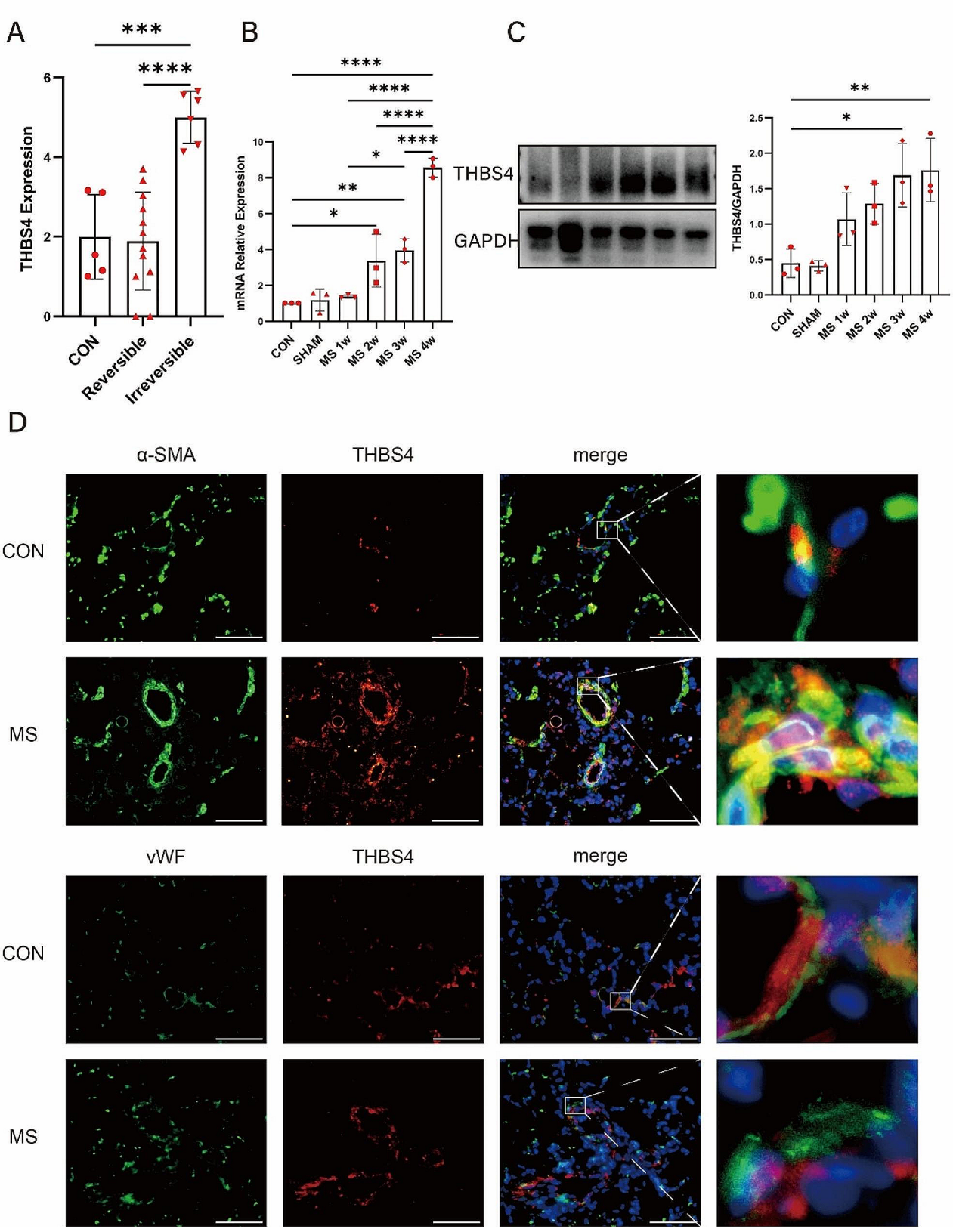

Fig. 4 Expression of THBS4 in PAH rats induced by MCT plus aorto-caval shunt. **(A)** THBS4 expression in GSE149899. qRT-PCR **(B)** and Western blot **(C)** showed the time course of THBS4 expression in PAH rats induced by MCT plus aorto-caval shunt. **(D)** Double immunofluorescence staining of THBS4 with α-SMA or VWF. Scare bars: 50 μm. CON: the control group; SHAM: the sham group; MS: PAH rats induced by MCT plus aorto-caval shunt (MS) from 1 week (1w) to 4 weeks (4w). The resultant data are represented as mean ± SD. $^{*}P < 0.05$; $^{**}P < 0.01$; $^{***}P < 0.001$; $^{****}P < 0.0001$

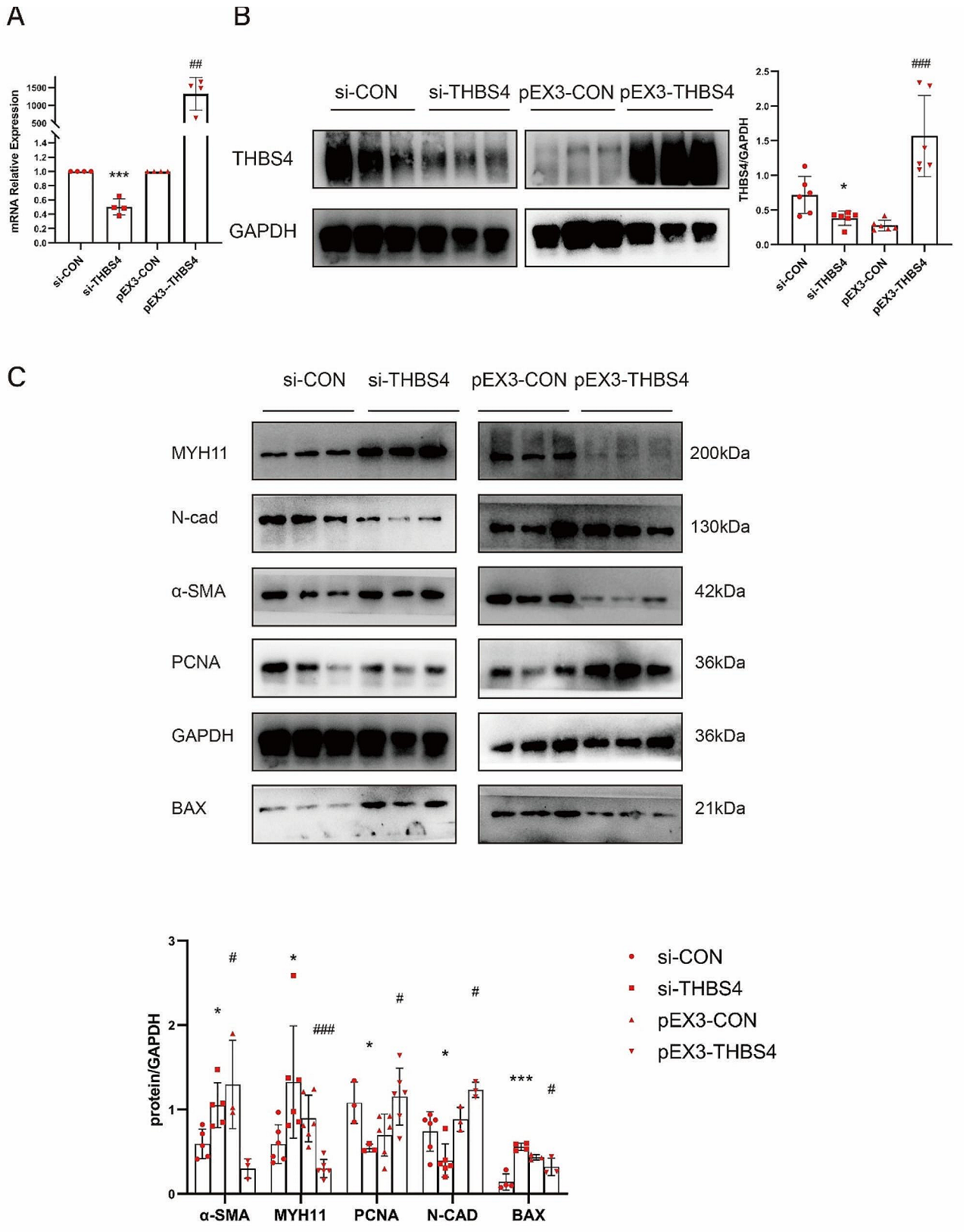

Fig. 5 qRT-PCR **(A)** and Western blot **(B)** showed the transfection efficiency of THBS4 in PASMCs. **(C)** The influence of THBS4 on the transformation of phenotype of PASMCs. The resultant data are represented as mean ± SD. *: si-THBS4 vs.si-CON; #: pEX3-THBS4 vs. pEX3-CON. $^{*}P < 0.05$; $^{***}P < 0.001$; $^{\#}P < 0.05$; $^{\#\#}P < 0.01$; $^{\#\#\#}P < 0.001$

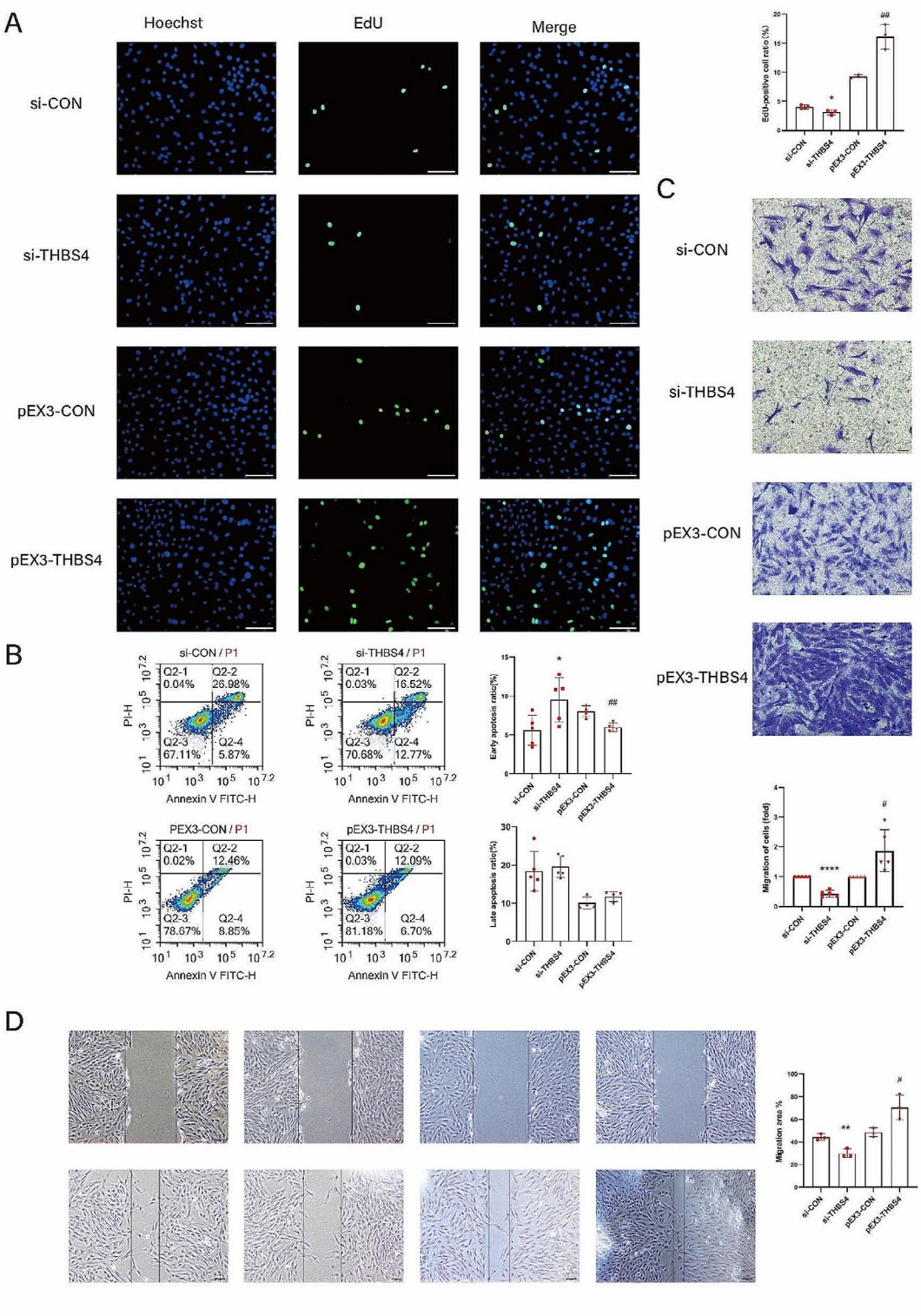

Fig. 6 Effect of THBS4 on the proliferation, apoptosis, and migration of PASMCs. **(A)** Effect of THBS4 on proliferation of PASMCs, as determined by the EdU assay. Scare bars, 100 μm. **(B)** Effect of THBS4 on apoptosis of PASMCs, as determined by the Annexin-V flow cytometry. **(C)** Effect of THBS4 on migration of PASMCs, as determined by the Wound healing assay. Scare bars, 200 μm. **(D)** Effect of THBS4 on migration of PASMCs, as determined by the Transwell assay. Scare bars, 100 μm. The resultant data are represented as mean ± SD. *: si-THBS4 vs.si-CON; #: pEX3-THBS4 vs. pEX3-CON. $^{*}P < 0.05$; $^{**}P < 0.01$; $^{****}P < 0.0001$; $^{\#}P < 0.05$; $^{\#\#}P < 0.01$

migration of PASMCs. When THBS4 was inhibited by siRNA, the number of migrated cells (0.4326±0.110 vs. 1.000±0.000, $P<0.0001$) and the percentage of migration area (29.99±3.886 vs. 44.31%±2.705, $P=0.0063$) are decreased. Conversely, When THBS4 was upregulated by plasmid transfection, the number of migrated cells (1.870±0.704 vs. 1.000±0.000, $P=0.0246$) and the percentage of migration area (70.43%±10.860 vs. 48.65%±3.888, $P=0.0308$) are decreased. Taken together, these results support that THBS4 promotes migraine of PASMCs.

Effect of THBS4 on the PI3K/AKT pathway

Given the fact that THBS4 contributed to tumor growth and progression through the PI3K/AKT pathway, and PI3K/AKT is involved in the progression of PAH by promoting proliferation, phenotype change, and migration of THBS4, we further investigated the effect of THBS4 on the PI3K/AKT pathway. Western blot (Fig. 7) showed that the phosphorylation level of PI3K and AKT elevated significantly in PASMCs when THBS4 is overexpressed, while it was reduced when THBS4 is inhibited. Nevertheless, the total level of PI3K and AKT were not changed significantly. Therefore, we assumed that the effect of THBS4 on PASMCs phenotype change, proliferation, and migration via the AKT/PI3K pathway.

THBS4 suppression ameliorates pulmonary vascular remodeling in MCT-AV rats

Since THBS4 promotes the proliferation, migration, and phenotype transformation of PASMCs while represses apoptosis in vitro, we next explore whether THBS4 has an influence on pulmonary vascular remodeling in vivo. The expression of THBS4 in the MCT-AV rat model was inhibited by intratracheal administration of AAV. The efficiency of AAV transfection was determined by detecting green fluorescence protein (Fig. 8A) that is encoded by AAV in lung tissues. Intratracheal administration of

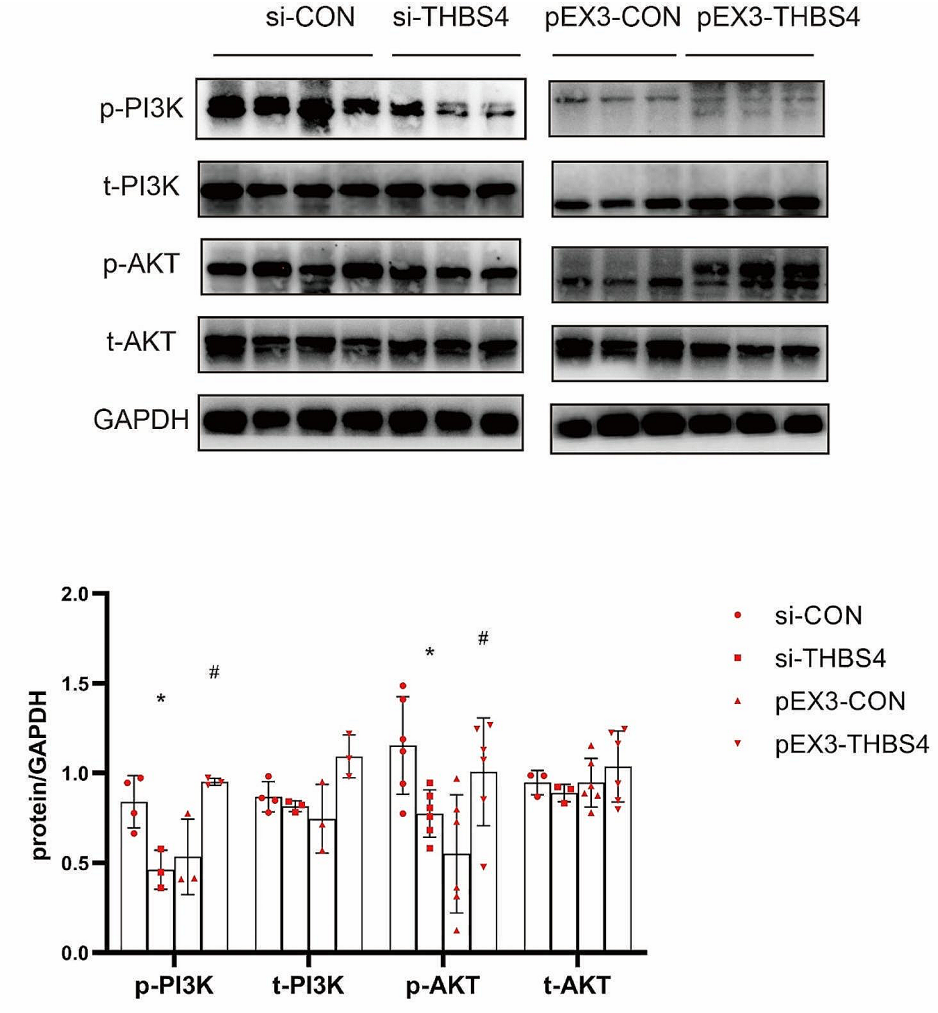

Fig. 7 Phosphorylation level of PI3K/AKT in PASMCs after inhibition and overexpression of THBS4 in PASMCs. The resultant data are represented as mean ± SD. *: si-THBS4 vs. si-CON; #: pEX3-THBS4 vs. pEX3-CON. $^{*}P<0.5$; $^{\#}P<0.5$

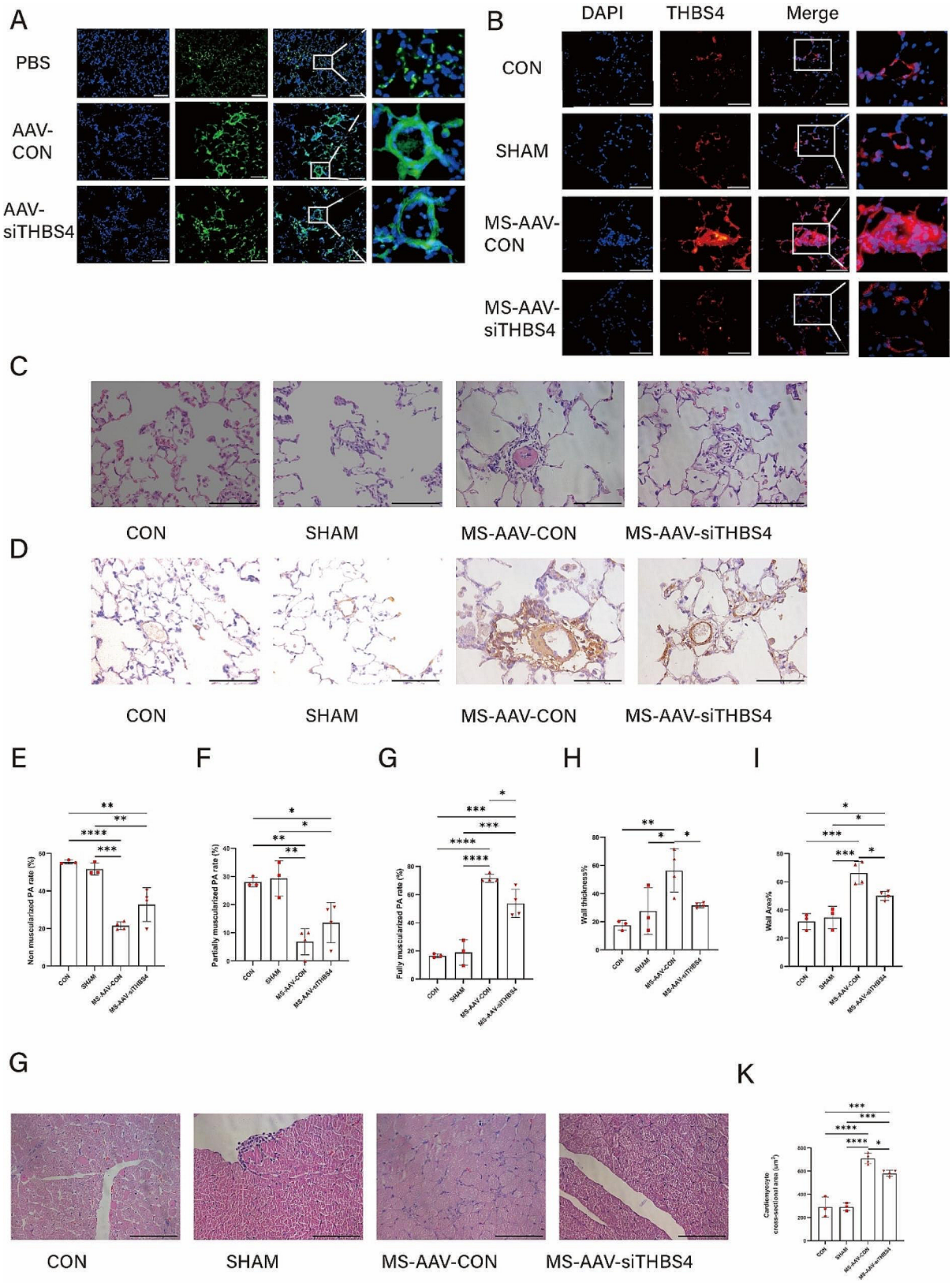

Fig. 8 (See legend on next page.)

(See figure on previous page.)

Fig. 8 Effect of THBS4 suppression on pulmonary vascular remodeling in PAH rats induced by MCT plus aorto-caval shunt. **(A)** The AAV transfection efficiency was determined by detecting green fluorescence protein which is encoded by AAV in lung tissues. Scare bars, 100 μm. **(B)** THBS4 suppression efficiency determined by immunofluorescence staining of THBS4. Scare bars, 50 μm. **(C)** Hematoxylin and Eosin staining of lung tissues. Scare bars,100 μm. **(D)** Immunofluorescence staining of α-SMA in lung tissues. Scare bars,100 μm. The percentage of non-muscularized **(E)**, partially-muscularized (F), and fully-muscularized pulmonary arterioles **(G)**. **(H)** The percentage of wall thickness. **(I)** The percentage of wall area. **(G)** Cross-sectional area of the right ventricular cardiomyocyte. Scare bars,100 μm. The resultant data are represented as mean ± SD. CON: control group; SHAM: sham group; MS-AAV-CON: administration of control AAV + MCT plus aorto-caval shunt induced PAH rats; MS-AAV-siTHBS4: administration of THBS4 suppression AAV + MCT plus aorto-caval shunt induced PAH rats. PA: pulmonary arteriole. $^{*}P < 0.05$; $^{**}P < 0.01$; $^{***}P < 0.001$; $^{****}P < 0.0001$

AAV resulted in stronger green fluorescence in the pulmonary artery compared to intratracheal administration of PBS. IF staining of THBS4 (Fig. 8B) further showed that THBS4 expression was effectively repressed in lung tissues of the MS-AAV-siTHBS4 group compared with in MS-AAV-siCON. HE staining (Fig. 8C) and IF staining against α-SMA (Fig. 8D) showed that THBS4 inhibition ameliorated the pulmonary vascular remodeling. Specifically, THBS4 attenuated thickened vascular wall, neointima lesion, and immune cell infiltration in MCT-AV rats. And the degree of muscularization of small pulmonary arterioles (Fig. 8E-G), the ratio of wall thickness (Fig. 8H), the ratio of wall area (Fig. 8I), and the cross sectional area of cardiomyocyte (Fig. 8J-K) were significantly reduced. In conclusion, THBS4 suppression ameliorates the vascular remodeling in MCT-AV rats.

Discussion

Here, we found that THBS4 is expressed in the pulmonary artery and upregulated in lung tissues of MCT-AV rats, and further upregulated in severe pulmonary vascular lesions. Furthermore, THBS4 was expressed mainly in PASMCs. THBS4 predisposes PASMC to a proliferative, apoptosis-resistant phenotype, potentiates proliferation and migration of PASMCs, and suppresses apoptosis. And the impact of THBS4 on PASMCs was achieved porbably through regulation of the phosphorylation level of PI3K/AKT pathway. THBS4 suppression attenuated pulmonary vascular remodeling and immune cell infiltration in MCT-AV rats. Compared with simple CHD and mild PAH-CHD, circulating levels of THBS4 in patients with severe PAH-CHD were significantly elevated. It is the first time that the expression and role of THBS4 in the pulmonary arteries and pulmonary vascular remodeling in PAH has been discovered. THBS4 is a promising biomarker to distinguish reversible pulmonary vascular lesion from irreversible in patients with PAH-CHD and a promising therapeutic target in PAH-CHD, especially when pulmonary vascular lesion is irreversible.

Due to its unique hemodynamics, pulmonary vascular disease in PAH-CHD can generally be reversed in an early phase, however, PAH-CHD with systemic-to-pulmonary shunt can ultimately become irreversible, closure of the shunt during this period will accelerate disease progression, as these patients have the worst prognosis among other types of PAH-CHD, even worse than patients with Eisenmanger syndrome [5–7]. Unfortunately, to date, no recognized and reliable assessments to distinguish these two stages are available before closure; moreover, the mechanism involved in the transition from the reversible to the irreversible stage is elusive. In this study, we found that THBS4 was upregulated in lung tissues of MCT-AV rat model, and further upregulated in severe pulmonary vascular lesions. Furthermore, the circulation level of THBS4 was obviously elevated in severe PAH-CHD. Hence, THBS4 is a promising biomarker to distinguish reversible pulmonary vascular lesion from irreversible in patients with PAH-CHD. As an invasive operation, lung biopsy is limited in clinical practice. Furthermore, in view of the patchy distribution of vascular lesions of the PAH, the negative result of lung biopsy does not rule out the likelihood of irreversible PAH-CHD. Hence, detection of THBS4 expression in lung tissues to decide the reversibility of PAH-CHD is limited. Therefore, the concentration of the circulating level of THBS4 is an ideal surrogate because it is readily available. Studies found that the circulating level of THBS4 was upregulated in peripheral arterial disease and positively associated with the severity of peripheral arterial disease. Additionally, the circulating THBS4 level was reduced after proper treatment [26, 27]. However, a larger sample size of patients is needed to guarantee the reliability of the results.

Targeted PAH therapies are proved to be effect and safe, and improve the hemodynamics, exercise capacity, and quality of life in PAH-CHD. However, PAH-CHD is associated with a poor outcome, especially when vascular lesions are irreversible. Previous studies showed that vascular endothelial cells and smooth muscle cells express THBS4. And THBS4 is generally localized on the outer side of the capillaries and in the adventitia of larger blood vessels [17]. Human endothelial cells and vascular smooth muscle cells from brain blood vessels and coronary arteries also express THBS4 and THBS4 improves proliferation of endothelial cells and vascular smooth muscle cells [18]. Studies in vitro and in vivo showed that THBS4 promotes vascular cell growth, angiogenesis, and vascular remodeling [17, 19–22]. Compared with wide-type mice, $THBS4^{-/-}$ mice showed reduced angiogenesis and reduced adhesion, migration, and proliferation of endothelial cells. Conversely, recombinant THBS4 promotes proliferation and migration of endothelial cells [17, 20]. In this study, we found that overexpression of THBS4

promotes the phenotype transformation, proliferation, migration, and inhibits apoptosis of PASMCs in vitro and ameliorate pulmonary vascular remodeling in vivo. Therefore, THBS4 is a promising target for treatment in patients with PAH-CHD, especially in its irreversible stage.

THBS4 also enhance macrophage infiltration and inflammatory cytokines in atherosclerotic lesions and tumor tissues [28, 29]. THBS4 is upregulated in atherosclerotic lesions and in areas prone to be atherosclerotic lesions and has an impact on recruitment of macrophages by activating endothelial cells and increasing adhesion and migration of macrophages [28]. Thbs4$^{-/-}$/ApoE$^{-/-}$ mice showed smaller atherosclerotic lesions, lower level of inflammatory cytokines, and less activated endothelial cells. Recombinant THBS4 increases adhesion and migration of macrophage and neutrophils, and activate inflammatory pathways. Here, we found that THBS4 suppression reduce immune cell infiltration in MCT-AV model. Given the fact that inflammation is one of the key factors involved in the progression of PAH and treatment targeted for inflammation ameliorates PAH [30, 31]. So suppression of inflammation is another reason why THBS4 may be a promising therapeutic target in PAH-CHD. However, we did not perform a quantitative analysis or specific classification of inflammatory cells. Hence, further studies are guaranteed.

The PI3K-AKT pathway play a vital role in cell metabolism, growth, proliferation, and survival [32]. Furthermore, the PI3K-AKT pathway mediates progression of PAH by promoting the proliferation, phenotype transformation, and migration of PASMCs [33–37]. PI3K-AKT is also one of the important mechanisms of THBS4 mediating tumor progression [14, 38, 39]. THBS4 overexpression favors proliferation and metastasis of hepatocellular carcinoma through the PI3K-AKT pathway [14]. THBS4 favors angiogenesis in gastric cancer through the PI3K-AKT pathway [38]. THBS4 also facilitates self-renewal and proliferation, curbs apoptosis of prostate cancer stem cells, and enhances in vivo tumorigenicity, which is achieved by activating the PI3K/AKT pathway [39]. Herein, we discovered that THBS4 inhibition decreases the phosphorylation level of PI3K and AKT. Conversely, THBS4 overexpression elevated the phosphorylation level of PI3K and AKT. Therefore, we speculate that THBS4 mediates the transformation of phenotype, the proliferation also the migration of PASMC through the PI3K-AKT pathway. However, in-depth studies are needed.

THBS4 was remarkably upregulated in a remodeled heart induced by increased ventricular load. THBS4 was upregulated in the late stage of diastolic heart failure that develops from hypertrophic hearts [40] in heart induced by chronic volume overload in the aorto-caval shunt [41], and in heart induced by pressure overload in Arginine8-vasopressin infusion or angiotensin II infusion [42]. THBS4 was also obviously increased in failure heart from patients [43, 44]. Therefore, the elevated concentration of THBS4 in plasma of severe PAH-CHD can be attributed to the remodeled pulmonary artery and remodeled right ventricle.

We acknowledge several limitations of this study. First, owing to the difficulty in obtaining lung tissues from patients with PAH-CHD, the expression of THBS4 is based on the MCT-AV rats model, which needs to be further verified in lung tissues from patients with PAH-CHD; Second, the mechanism involved in the influence of THBS4 on phenotype, proliferation, apoptosis, and migration of PASMCs was unclear and needs further investigation; Third, a larger sample size of patients with PAH-CHD is needed to guarantee the reliability of circulating THBS4 in distinguishing reversible from irreversible PAH-CHD.

Conclusions

THBS4 is a promising biomarker to distinguish reversible from irreversible PAH-CHD before repairing the shunt. THBS4 is a potential treatment target in PAH-CHD, especially in irreversible stage.

Abbreviations

AAV	Adeno-associated virus
AV	Aorto-caval shunt
CHD	Congenital heart disease
ED	External diameter
FBS	Fetal bovine serum
HE	Hematoxylin and Eosin
IF	Immunofluorescence
IHC	Immunohistochemistry
LA	Lumen area
LD	Lumen diameter
MCT	Monocrotaline
PAH	Pulmonary arterial hypertension
PAH-CHD	Pulmonary arterial hypertension associated with congenital heart disease
PASMC	Primary pulmonary artery smooth muscle cell
RVHI	Right heart hypertrophy index
RVSP	Right ventricular systolic pressure
TA	Total area
THBS4	Thrombospondin-4
WA	Wall area
WT	Wall thickness

Supplementary Information

The online version contains supplementary material available at https://doi.org/10.1186/s12931-024-02932-w.

Supplementary Material 1: Figure 1 Pulmonary smooth muscle cell identification by immunofluorescence staining against α-SMA

Supplementary Material 2

Author contributions

HW Z and YS Z conceived and designed the study; HW Z, BD L, BY L, and H X performed aorto-caval shunt surgery and hemodynamic measurements.

HW Z, BD L, EF Z, XQ L, XY X, JY S, and LJ S performed the in vitro experiment. HW Z, and YS Z wrote the first draft. All authors reviewed and edited the manuscript. All authors read and approved the final manuscript.

Funding
Not applicable.

Data availability
No datasets were generated or analysed during the current study.

Declarations

Ethics approval and consent to participate
All protocols in animal studies and patients were approved by the Ethics Committee of Xi'an Jiaotong University (No. 2021 – 1510). All patients signed an informed consent. All patients consented to participate in this study.

Consent for publication
Not Applicable.

Competing interests
The authors declare no competing interests.

Author details
[1]Department of Cardiovascular Surgery, the First Affiliated Hospital of Xi'an Jiaotong University, Xi'an, China
[2]Department of Ultrasound, the First Affiliated Hospital of Anhui Medical University, Hefei 230022, Anhui Province, China

Received: 14 April 2024 / Accepted: 31 July 2024
Published online: 17 August 2024

References

1. Humbert M, Kovacs G, Hoeper MM, Badagliacca R, Berger RMF, Brida M, Carlsen J, Coats AJS, Escribano-Subias P, Ferrari P, et al. 2022 ESC/ERS guidelines for the diagnosis and treatment of pulmonary hypertension. Eur Heart J. 2022;43:3618–731.
2. van Riel AC, Schuuring MJ, van Hessen ID, Zwinderman AH, Cozijnsen L, Reichert CL, Hoorntje JC, Wagenaar LJ, Post MC, van Dijk AP, et al. Contemporary prevalence of pulmonary arterial hypertension in adult congenital heart disease following the updated clinical classification. Int J Cardiol. 2014;174:299–305.
3. Lammers AE, Bauer LJ, Diller GP, Helm PC, Abdul-Khaliq H, Bauer UMM, Baumgartner H. Pulmonary hypertension after shunt closure in patients with simple congenital heart defects. Int J Cardiol. 2020;308:28–32.
4. van Loon RL, Roofthooft MT, Hillege HL, ten Harkel AD, van Osch-Gevers M, Delhaas T, Kapusta L, Strengers JL, Rammeloo L, Clur SA, et al. Pediatric pulmonary hypertension in the Netherlands: epidemiology and characterization during the period 1991 to 2005. Circulation. 2011;124:1755–64.
5. Wagenvoort CA, Wagenvoort N, Draulans-Noë Y. Reversibility of plexogenic pulmonary arteriopathy following banding of the pulmonary artery. J Thorac Cardiovasc Surg. 1984;87:876–86.
6. D'Alto M, Romeo E, Argiento P, Correra A, Santoro G, Gaio G, Sarubbi B, Calabrò R, Russo MG. Hemodynamics of patients developing pulmonary arterial hypertension after shunt closure. Int J Cardiol. 2013;168:3797–801.
7. Manes A, Palazzini M, Leci E, Bacchi Reggiani ML, Branzi A, Galiè N. Current era survival of patients with pulmonary arterial hypertension associated with congenital heart disease: a comparison between clinical subgroups. Eur Heart J. 2014;35:716–24.
8. Förster S, Gretschel S, Jöns T, Yashiro M, Kemmner W. THBS4, a novel stromal molecule of diffuse-type gastric adenocarcinomas, identified by transcriptome-wide expression profiling. Mod Pathol. 2011;24:1390–403.
9. Chen X, Huang Y, Wang Y, Wu Q, Hong S, Huang Z. THBS4 predicts poor outcomes and promotes proliferation and metastasis in gastric cancer. J Physiol Biochem. 2019;75:117–23.
10. Kuroda K, Yashiro M, Sera T, Yamamoto Y, Kushitani Y, Sugimoto A, Kushiyama S, Nishimura S, Togano S, Okuno T, et al. The clinicopathological significance of Thrombospondin-4 expression in the tumor microenvironment of gastric cancer. PLoS ONE. 2019;14:e0224727.
11. Dakhova O, Ozen M, Creighton CJ, Li R, Ayala G, Rowley D, Ittmann M. Global gene expression analysis of reactive stroma in prostate cancer. Clin Cancer Res. 2009;15:3979–89.
12. Liu J, Cheng G, Yang H, Deng X, Qin C, Hua L, Yin C. Reciprocal regulation of long noncoding RNAs THBS4–003 and THBS4 control migration and invasion in prostate cancer cell lines. Mol Med Rep. 2016;14:1451–8.
13. Su F, Zhao J, Qin S, Wang R, Li Y, Wang Q, Tan Y, Jin H, Zhu F, Ou Y, et al. Over-expression of Thrombospondin 4 correlates with loss of miR-142 and contributes to migration and vascular invasion of advanced hepatocellular carcinoma. Oncotarget. 2017;8:23277–88.
14. Guo D, Zhang D, Ren M, Lu G, Zhang X, He S, Li Y. THBS4 promotes HCC progression by regulating ITGB1 via FAK/PI3K/AKT pathway. Faseb j. 2020;34:10668–81.
15. Chou KY, Chang AC, Ho CY, Tsai TF, Chen HE, Chen PC, Hwang TI. Thrombospondin-4 promotes bladder cancer cell migration and invasion via MMP2 production. J Cell Mol Med. 2021;25:6046–55.
16. Wu H, Zhang G, Li Z, Ma J, Han X, Xiang T, Jiang X. Thrombospondin-4 expression as a prognostic marker in hepatocellular carcinoma. Gene. 2019;696:219–24.
17. Muppala S, Frolova E, Xiao R, Krukovets I, Yoon S, Hoppe G, Vasanji A, Plow E, Stenina-Adognravi O. Proangiogenic properties of Thrombospondin-4. Arterioscler Thromb Vasc Biol. 2015;35:1975–86.
18. Stenina OI, Desai SY, Krukovets I, Kight K, Janigro D, Topol EJ, Plow EF. Thrombospondin-4 and its variants: expression and differential effects on endothelial cells. Circulation. 2003;108:1514–9.
19. Frolova EG, Sopko N, Blech L, Popovic ZB, Li J, Vasanji A, Drumm C, Krukovets I, Jain MK, Penn MS, et al. Thrombospondin-4 regulates fibrosis and remodeling of the myocardium in response to pressure overload. Faseb j. 2012;26:2363–73.
20. Muppala S, Xiao R, Krukovets I, Verbovetsky D, Yendamuri R, Habib N, Raman P, Plow E, Stenina-Adognravi O. Thrombospondin-4 mediates TGF-β-induced angiogenesis. Oncogene. 2017;36:5189–98.
21. Frolova EG, Drazba J, Krukovets I, Kostenko V, Blech L, Harry C, Vasanji A, Drumm C, Sul P, Jenniskens GJ, et al. Control of organization and function of muscle and tendon by thrombospondin-4. Matrix Biol. 2014;37:35–48.
22. Ge H, Shrestha A, Liu C, Wu P, Cheng B. MicroRNA 148a-3p promotes Thrombospondin-4 expression and enhances angiogenesis during tendinopathy development by inhibiting Krüppel-like factor 6. Biochem Biophys Res Commun. 2018;502:276–82.
23. Ritchie ME, Phipson B, Wu D, Hu Y, Law CW, Shi W. Smyth GK: limma powers differential expression analyses for RNA-sequencing and microarray studies. Nucleic Acids Res. 2015;43:e47.
24. van der Feen DE, Weij M, Smit-van Oosten A, Jorna LM, Hagdorn QA, Bartelds B, Berger RM. Shunt surgery, Right Heart catheterization, and vascular morphometry in a rat model for Flow-induced pulmonary arterial hypertension. J Vis Exp 2017.
25. Savai R, Al-Tamari HM, Sedding D, Kojonazarov B, Muecke C, Teske R, Capecchi MR, Weissmann N, Grimminger F, Seeger W, et al. Pro-proliferative and inflammatory signaling converge on FoxO1 transcription factor in pulmonary hypertension. Nat Med. 2014;20:1289–300.
26. Yazman S, Depboylu BC, Saruhan E, Cenikli U, Harmandar B, Arslan K, İlhan G, İştar H. New biomarkers (Endocan, Interleukin-17, and Thrombospondin-4) for the diagnosis, Assessment of Severity, and Follow-Up of peripheral arterial disease. Angiology. 2023;74:631–9.
27. Zierfuss B, Höbaus C, Herz CT, Pesau G, Koppensteiner R, Schernthaner GH. Thrombospondin-4 increases with the severity of peripheral arterial disease and is associated with diabetes. Heart Vessels. 2020;35:52–8.
28. Frolova EG, Pluskota E, Krukovets I, Burke T, Drumm C, Smith JD, Blech L, Febbraio M, Bornstein P, Plow EF, Stenina OI. Thrombospondin-4 regulates vascular inflammation and atherogenesis. Circ Res. 2010;107:1313–25.
29. Muppala S, Xiao R, Gajeton J, Krukovets I, Verbovetskiy D, Stenina-Adognravi O. Thrombospondin-4 mediates hyperglycemia- and TGF-beta-induced inflammation in breast cancer. Int J Cancer. 2021;148:2010–22.
30. Hassoun PM, Mouthon L, Barberà JA, Eddahibi S, Flores SC, Grimminger F, Jones PL, Maitland ML, Michelakis ED, Morrell NW, et al. Inflammation, growth factors, and pulmonary vascular remodeling. J Am Coll Cardiol. 2009;54:S10–9.
31. Pullamsetti SS, Savai R, Janssen W, Dahal BK, Seeger W, Grimminger F, Ghofrani HA, Weissmann N, Schermuly RT. Inflammation, immunological reaction and role of infection in pulmonary hypertension. Clin Microbiol Infect. 2011;17:7–14.

32. Hers I, Vincent EE, Tavaré JM. Akt signalling in health and disease. Cell Signal. 2011;23:1515–27.
33. Fan Z, Li C, Qin C, Xie L, Wang X, Gao Z, Qiangbacuozhen, Wang T, Yu L, Liu H. Role of the PI3K/AKT pathway in modulating cytoskeleton rearrangements and phenotype switching in rat pulmonary arterial vascular smooth muscle cells. DNA Cell Biol. 2014;33:12–9.
34. Huang H, Kong L, Luan S, Qi C, Wu F. Ligustrazine suppresses platelet-derived growth Factor-BB-Induced Pulmonary artery smooth muscle cell proliferation and inflammation by regulating the PI3K/AKT signaling pathway. Am J Chin Med. 2021;49:437–59.
35. Tian H, Liu L, Wu Y, Wang R, Jiang Y, Hu R, Zhu L, Li L, Fang Y, Yang C, et al. Resistin-like molecule β acts as a mitogenic factor in hypoxic pulmonary hypertension via the ca(2+)-dependent PI3K/Akt/mTOR and PKC/MAPK signaling pathways. Respir Res. 2021;22:8.
36. Zhang S, Wang J, Qi X, Tao X, Xie W, Wan J, Shen YH, Zhai Z. Plasminogen activator Inhibitor-2 inhibits pulmonary arterial smooth muscle cell proliferation in pulmonary arterial hypertension via PI3K/Akt and ERK signaling. Exp Cell Res. 2021;398:112392.
37. Zhou J, Li F, Yang Y. Protective effects of calcyclin-binding protein against pulmonary vascular remodeling in flow-associated pulmonary arterial hypertension. Respir Res. 2022;23:223.
38. He L, Wang W, Shi H, Jiang C, Yao H, Zhang Y, Qian W, Lin R. THBS4/integrin α2 axis mediates BM-MSCs to promote angiogenesis in gastric cancer associated with chronic Helicobacter pylori infection. Aging. 2021;13:19375–96.
39. Hou Y, Li H, Huo W. THBS4 silencing regulates the cancer stem cell-like properties in prostate cancer via blocking the PI3K/Akt pathway. Prostate. 2020;80:753–63.
40. Rysä J, Leskinen H, Ilves M, Ruskoaho H. Distinct upregulation of extracellular matrix genes in transition from hypertrophy to hypertensive heart failure. Hypertension. 2005;45:927–33.
41. Melenovsky V, Benes J, Skaroupkova P, Sedmera D, Strnad H, Kolar M, Vlcek C, Petrak J, Benes J Jr., Papousek F, et al. Metabolic characterization of volume overload heart failure due to aorto-caval fistula in rats. Mol Cell Biochem. 2011;354:83–96.
42. Mustonen E, Aro J, Puhakka J, Ilves M, Soini Y, Leskinen H, Ruskoaho H, Rysä J. Thrombospondin-4 expression is rapidly upregulated by cardiac overload. Biochem Biophys Res Commun. 2008;373:186–91.
43. Tan FL, Moravec CS, Li J, Apperson-Hansen C, McCarthy PM, Young JB, Bond M. The gene expression fingerprint of human heart failure. Proc Natl Acad Sci U S A. 2002;99:11387–92.
44. Gabrielsen A, Lawler PR, Yongzhong W, Steinbrüchel D, Blagoja D, Paulsson-Berne G, Kastrup J, Hansson GK. Gene expression signals involved in ischemic injury, extracellular matrix composition and fibrosis defined by global mRNA profiling of the human left ventricular myocardium. J Mol Cell Cardiol. 2007;42:870–83.

Publisher's Note